Available online at www.sciencedirect.com
ScienceDirect
Journal of Nuclear Materials 372 (2008) 249–255
journal of nuclear materials
www.elsevier.com/locate/jnucmat

Measurement of the Young modulus anisotropy of a reactor pressure vessel cladding

W. Vandermeulen [a], M. Scibetta [a,*], A. Leenaers [a], J. Schuurmans [a], R. Gérard [b]

[a] SCK-CEN, Boeretang 200, B-2400 Mol, Belgium
[b] Tractebel Engineering, Ariane Avenue 7, B-1200 Brussels, Belgium

Received 6 November 2006; accepted 20 March 2007

Abstract

The dynamic elastic modulus for directions in the plane of the cladding of a reactor pressure vessel was found to have an unusual low value of 165 GPa. In order to examine this phenomenon further, a cantilever bend test method was developed which allowed measuring the modulus along any desired direction relative to the cladding. It was found that in the as-clad as well as in the clad-and-annealed condition the deviations of the modulus from the bulk modulus depend on the orientation. The modulus values range from 145 GPa perpendicular to the cladding plane to 219 GPa at an angle of 35° to the cladding plane. These deviations from the bulk value are explained by the texture resulting from the directional heat flow during solidification and by the presence of the δ phase.

1. Introduction

The inner surface of a reactor pressure vessel, RPV, is covered with an austenitic stainless steel cladding to protect the ferritic steel of the vessel against corrosion and to avoid polluting the coolant with activated corrosion products. The cladding also plays a minor role in heat transfer damping, attenuation of radiation embrittlement and structural integrity. A study to investigate the mechanical properties of the cladding that have an impact on the safety assessment of the vessel was undertaken on a section of the RPV of the Lemoniz 1 unit. Lemoniz is a Spanish 900 MW Pressurized Water Reactor, the construction of which has been cancelled.

One of the characterization tests consisted of the determination of the dynamic elastic modulus with the impulse excitation method [1] in the longitudinal (L) and transverse (T) orientation of the base metal. In these directions, values around 165 GPa were obtained while 192–200 GPa are common values for austenitic steels [2,3]. These low values were also observed in the NESC project [4] and the occurrence of a texture [5,6] or the presence of the δ phase were considered as possible causes. The aim of the present study was to investigate these possibilities.

Ultrasonic techniques are generally used to determine the elastic constants of bulk materials. Isotropic structures as well as single crystals and anisotropic structures such as welds have been examined [7–10]. Unfortunately, some trial measurements were not conclusive. Therefore, it was attempted to determine the static modulus from small cantilever bending specimens. In the following, the experimental technique is described and the accuracy of the method is evaluated. Subsequently the method used to estimate the texture from simple X-ray diffraction patterns is given and the moduli for a perfect texture (single crystal) are calculated. Finally, the experimental results obtained on as-clad and clad-and-annealed material are given and the effects of texture and δ phase are discussed as possible causes of the modulus anisotropy.

2. Material

The material under investigation is a block extracted from the beltline region of the pressure vessel. The cladding

* Corresponding author. Tel.: +32 14333043; fax: +32 14333333.
E-mail address: mscibetta@sckcen.be (M. Scibetta).

0022-3115/$ - see front matter © 2007 Published by Elsevier B.V.
doi:10.1016/j.jnucmat.2007.03.213

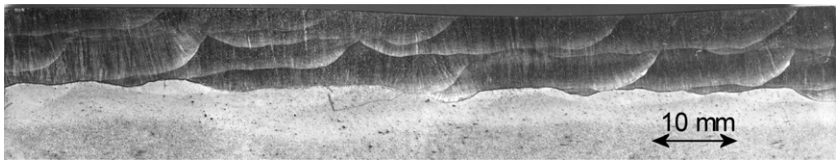

Fig. 1. Cross-section of the cladding. From top to bottom three zones can be identified: top layer, bottom layer and base metal.

Table 1
Chemical analysis on the cladding layers (weight%)

	C	Mn	Si	S	P	Cr	Ni	Mo	V	Cu	Co
Bottom layer	0.045	2.083	0.760	0.005	0.014	21.4	10.7	0.080	0.017	0.023	0.067
Top layer	0.071	1.767	0.720	0.005	0.014	19.6	9.7	0.157	0.020	0.030	0.030

was deposited in two layers of about 4.5 mm thick each. The weld beads, with a width of about 18 mm, were deposited in the L direction of the base plate. Fig. 1 shows a cross-section of the cladding perpendicular to the deposition direction. Chemical analyses were performed on both layers using spark emission spectrometry. The average results are given in Table 1. The composition corresponds with AISI 308 steel. Previous Feritscope MP30 measurements showed the presence of 7 vol% of the δ phase.

3. Experimental methods

3.1. Test specimen – test set-up

The set-up corresponds to the well-known cantilever beam for which analytical solutions for stress and deflection are available. The shape of the specimen is shown in Fig. 2. It consists of a test section (the cantilever beam) of nominally 0.8 by 2 by 8 mm, which forms a single part with a 'gripping' section. The test section always consists of the cladding material. The gripping section may consist of the cladding or the base metal. The fabrication is done by conventional machining. For the test, the specimen is clamped horizontally along the gripping section with the smallest dimension of the beam vertically. Loading is done by hanging a dead weight at the end of the beam (Fig. 3). In order to have a well-defined contact point the fixture of the dead weight rests on a 1 mm diameter steel ball which is fixed to the specimen with a low melting point solder. The deflection is measured by means of a displacement transducer (LVDT) which contacts the specimen below the loading point.

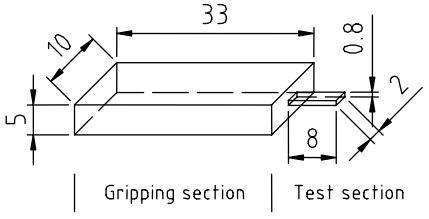

Fig. 2. Shape and dimensions (mm) of the test piece used for the bending tests.

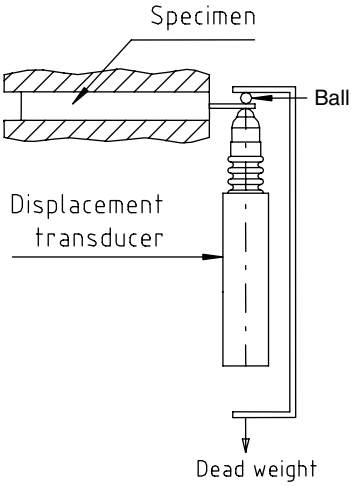

Fig. 3. Schematic test set-up.

3.2. Modulus calculation from the deflection

The E modulus was calculated from the formula giving the deflection of a beam with a rectangular cross-section, clamped at one end and loaded by a point force at the other end [11]:

$$E = F \cdot P \cdot L^3 / 3f \cdot I \quad (1)$$

with F, a factor taking into account the interface rotation at the clamped end [12]; P, the applied force; L, the distance of the loading point to the clamped end; f, the deflection and I, the moment of inertia of the cross-section.

3.3. Methodology of the bend tests

3.3.1. Dimensional measurements and LVDT calibration

Because of the small dimensions of the test section, dimensional measurements are critical for the final accuracy. From an estimation of the accuracy of the different measurements, it is concluded that a maximum error of 5% on the modulus can be expected. The LVDT was calibrated before each set of measurements by means of an

Instron calibrator allowing displacement control to 1 μm. The accuracy of the specimen deflection measurement is limited by the resolution of the instrument reading, which is about ±0.5 μm. This results in an error on the modulus of less than 1.3%.

3.3.2. Test execution

After mounting the specimen and the LVDT, the specimen is loaded by means of a dead weight (0.6–1 kg). The deflection is measured for at least five loading–unloading cycles and the modulus is calculated from the average deflection according to Eq. (1). The bending stresses are between 250 and 350 MPa. The highest value is slightly higher than the 0.2% yield stress for the L and T directions.

As a test of the accuracy of the method and in order to investigate the effect of the relatively high bending stresses used, tests were executed on two annealed stainless steel AISI304 specimens. These were tested with three different bending forces, giving bending stresses of 193, 243 and 327 MPa. The results will be discussed later.

3.4. Annealing treatment and dynamic modulus determination

In order to examine the effect of the δ phase all the specimens were wrapped in a stainless steel foil and annealed in air for 2.5 h at 1050 °C to dissolve the δ phase. Cooling was done slowly in the furnace. In addition to the static bend tests the dynamic modulus in the L (2 samples) and T (1 sample) directions was measured on $8 \times 8 \times 50$ mm^3 specimens by means of the impulse excitation method [1]. These specimens contain both cladding layers. They were tested in the as-clad condition and after the same annealing treatment as described above. For the test, they were oriented such that vibration occurred perpendicular to the cladding plane.

3.5. Texture estimation from X-ray diffraction

X-ray diffraction (XRD) patterns were recorded on a Philips X'Pert θ–θ diffractometer equipped with a Cu tube, configured in the standard Bragg-Brentano geometry. Scans of the diffraction peaks in the 30°–130° 2θ range were recorded with the X'Celerator, an area detector based on real time multiple strip (RTMS) technology. For all diffraction patterns, care was taken to use an X-ray beam of much larger cross-section than the average grain size (50 μm) in order to guarantee a representative pattern. From each sample, two diffraction patterns were made and the peak intensities were averaged.

4. Texture determination and anisotropy of the elastic modulus

4.1. Texture determination

For the description of the texture, the L, T and S directions of the base metal will be taken as the reference system. The texture was estimated from the XRD patterns of the cladding upper and lower layers along the L–T plane and of the upper layer along the T–S plane as shown in Fig. 4. The presence of austenite (γ) and ferrite (δ) diffraction peaks can be observed and the Miller indices of the peaks are given in Fig. 4(a). Table 2 shows the relative peak intensities of both phases for the three pattern sets. The relative peak intensities for the powders of austenitic stainless steel (ICDD 33-0397) and of pure iron (ICDD 6-0696) have been included for comparison. For the austenite, it can be seen that for both samples along the L–T plane the (200) peak is the most intense. For the top layer this is strongly pronounced but the bottom layer also shows a significant intensity of the (111) peak. For the ferrite the top layer also shows the dominance of the (200) peak while in the bottom layer the relative peak intensities are similar to the powder data. The XRD pattern of the top layer T–S section shows the dominance of the (220) austenite peak with a somewhat weaker contribution of the (200) peak. For this section the (110) ferrite peak dominates similarly to the powder data.

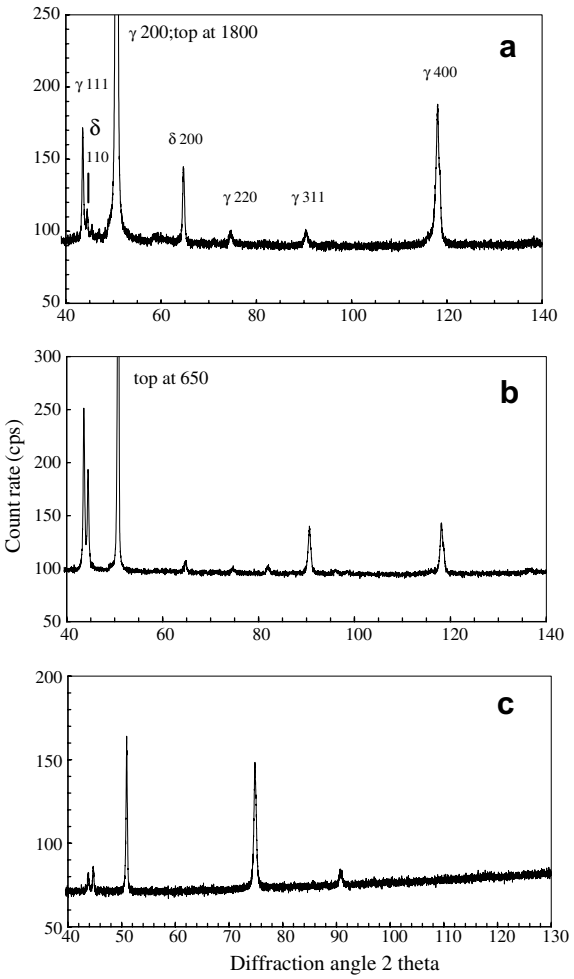

Fig. 4. Diffraction pattern of: (a) top layer, L–T plane, (b) bottom layer, L–T plane, (c) top layer, T–S plane.

Table 2
X-ray peak intensities for austenite and ferrite

Phase	hkl	Powder	L–T plane top layer	L–T plane bottom layer	T–S plane top layer
Austenite	111	100	4	28	16
	200	45	100	100	98
	220	26	1	1	100
	311	30	0	8	20
	222	12	0	0	0
	400	3	4	9	6
Ferrite	110	100	50	100	100
	200	20	100	11	0
	211	30	0	5	0
	220	10	0	0	0
	310	12	0	3	0
	222	6	0	0	0

As-clad condition.

From these observations, it follows that in the top layer there is a strong tendency of the ⟨100⟩ directions for being parallel with the S direction and that furthermore, in the plane of the cladding, there is a preference of the ⟨110⟩ directions for being parallel with the L direction. This applies to both austenite and ferrite. In the bottom layer the austenite maintains the same texture, although less pronounced. The ferrite peak intensities follow the powder data showing that in this layer the ferrite texture is weak. The dominating orientation of the austenite unit cell in the cladding is shown in Fig. 5.

Fig. 6 shows a T–S section of the cladding. It can be seen that growth of the δ phase has occurred mainly parallel to the S direction, which supports the existence of a texture.

4.2. Calculation of the modulus for a perfect texture

For austenitic stainless steels the isotropic modulus is reported to be 192–200 GPa [2,3]. An extreme texture leads to a material which becomes elastically equivalent to a single crystal. For most metals, the Young modulus of single crystals depends on the crystallographic direction considered. For cubic crystals, it can be calculated for a particular direction using the three elastic constants.

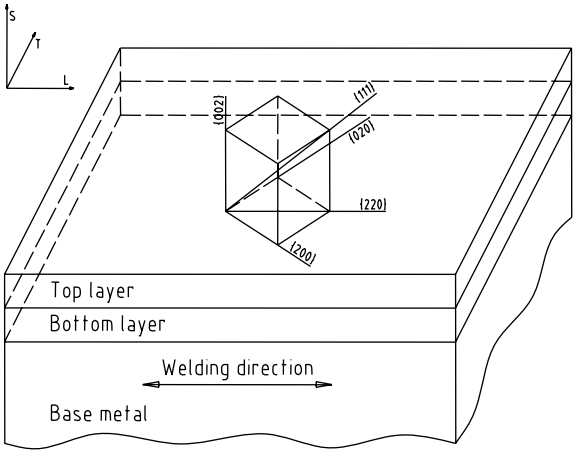

Fig. 5. Schematic representation of the dominant (cubic) crystal texture relative to the cladding and the base plate.

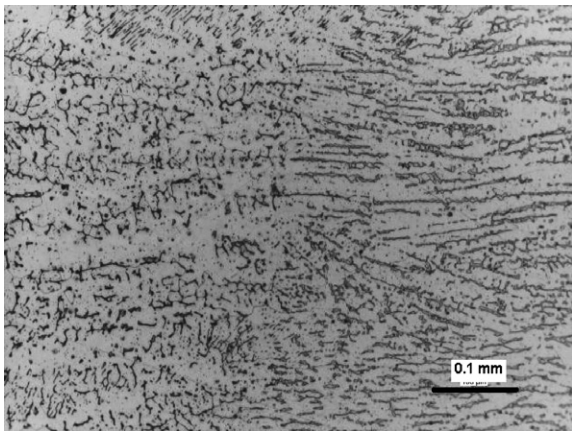

Fig. 6. Metallographic section along the T–S plane, showing the pronounced directionality evidenced by the δ phase morphology. The S direction is horizontal in the plane of the picture.

Ledbetter [7] gives the following values for the elastic stiffness constants of AISI 316 stainless steel:

$$C_{33} = C_{22} = C_{11} = 2.06 \times 10^{11}\ \mathrm{N/m^2},$$
$$C_{23} = C_{13} = C_{12} = 1.33 \times 10^{11}\ \mathrm{N/m^2},$$
$$C_{66} = C_{55} = C_{44} = 1.19 \times 10^{11}\ \mathrm{N/m^2}.$$

From the relationship between the elastic stiffness and the elastic compliance coefficients [13] the elastic compliance coefficients were calculated, giving

$$S_{33} = S_{22} = S_{11} = 9.84 \times 10^{-12}\ \mathrm{m^2/N},$$
$$S_{12} = -3.86 \times 10^{-12}\ \mathrm{m^2/N},$$
$$S_{44} = 8.40 \times 10^{-12}\ \mathrm{m^2/N}.$$

For a cubic crystal, the elastic modulus, E_{hkl}, corresponding to direction hkl, is given by [13]

$$1/E_{hkl} = S_{11} - 2[(S_{11} - S_{12}) - S_{44}/2]\,(l^2m^2 + m^2n^2 + l^2n^2), \quad (2)$$

where l, m, n are the direction cosines of direction hkl.

Using Eq. (2), the moduli for the ⟨100⟩, ⟨110⟩ and ⟨111⟩ directions were found to be respectively 102, 196 and 285 GPa. Since the modulus of austenitic steels is nearly independent of composition [2,3] it may safely be assumed that these moduli, based on the elastic constants of AISI316, are also valid for the present type AISI308 cladding material. From the values above, it can be seen that the ⟨100⟩ and ⟨110⟩ directions, which have been found to be dominantly parallel with the L, T, or S directions, have a low to normal modulus. The ⟨111⟩ direction has a high modulus. From Fig. 5 it can be seen that one of the ⟨111⟩ directions makes an angle of 35° with the plane

of the cladding and lies in the *LS* plane. In the following this macroscopic direction will be indicated by ⟨1 1 1⟩ in order to differentiate it from the crystallographic ⟨1 1 1⟩ direction.

5. Results of the bend tests

5.1. Accuracy of the method

The tests on AISI304 steel, for which bending stresses between 193 and 327 MPa were used, yielded modulus values from 196 to 199 GPa. These values are well within the range cited in data compilations [2,3] and confirm the estimated accuracy. Moreover, the small spread shows that within the above mentioned range the bending stress does not affect the measurement.

5.2. Tests on the as-clad material

The moduli, measured in the *L*, *T*, *S* and ⟨1 1 1⟩ directions, are given in Table 3, column 3. The averages for each direction are given in column 4. The test stresses for each sample are shown in column 5.

The data show that the moduli in the *L*, *T* and *S* directions are smaller than the isotropic bulk modulus (195 GPa) while the modulus in the ⟨1 1 1⟩ direction is larger.

Although no correlation was found between the test stresses and the modulus values the possible effect of plastic deformation was examined on one specimen. After measuring the modulus in the as-clad condition, the full test-section was bent deliberately to a radius of curvature of about 20 mm and straightened again. This bending caused a plastic strain of 2% at the surface. The modulus was measured again after straightening. No significant difference was found.

5.3. Tests on the annealed cladding

Since during the annealing treatment the texture might have changed due to recrystallisation, the samples used for XRD were annealed as well. New diffractograms showed no significant change of the relative austenite peak intensities. Metallographic examination showed that most of the ferrite has been dissolved after annealing (Fig. 7). This figure also confirms the absence of recrystallisation by the wavy aspect of the grain boundaries – a characteristic of the solidification structure – and by the absence of annealing twins.

The individual bend test results, their averages and the test stresses are shown in Table 3 (columns 6–8). It can be seen that for the *L*, *T* and *S* directions, annealing causes the difference between the as-clad values and the bulk value to decrease by roughly 50%. For the ⟨1 1 1⟩ direction annealing has no effect. Again, no correlation is observed between the test stress and the modulus value.

The results obtained with the impulse excitation method for the *L* and *T* directions before and after annealing are also included in Table 3. In the as-clad condition the moduli obtained are similar to those obtained with the bending method. However, in contrast to the static bend tests no significant change upon annealing is observed.

In Fig. 8 the average moduli for the bulk [2,3], the measured as-clad, the measured clad-and-annealed, and the calculated single-crystal conditions are compared for the different specimen orientations. It can be seen that going

Table 3
Test results

Specimen orientation	Specimen number	Modulus as-clad (GPa)	Modulus average (GPa)	Test stress (MPa)	Modulus annealed (GPa)	Modulus average (GPa)	Test stress (MPa)
L	3	156		340	165		340
	L02	175		344	192		296
	L03	173		352	176		318
	L04	168	168	334	182	179	303
	46E8	169[a]			169[a]		
	46D31	163[a]			161[a]		
T	1	182		328	188		344
	T02	170		350	188		314
	T03	178		328	191		302
	T04	161	173	347	185	188	314
	24	168[a]			170[a]		
S	2	144		312	167		320
	S02	125		266	175		258
	S03	160		290	183		273
	S04	152	145	297	171	174	307
⟨1 1 1⟩	35–1	215		300	216		307
	35–2	226		299	229		312
	35–3	215	219	306	219	221	298

[a] Impulse excitation results.

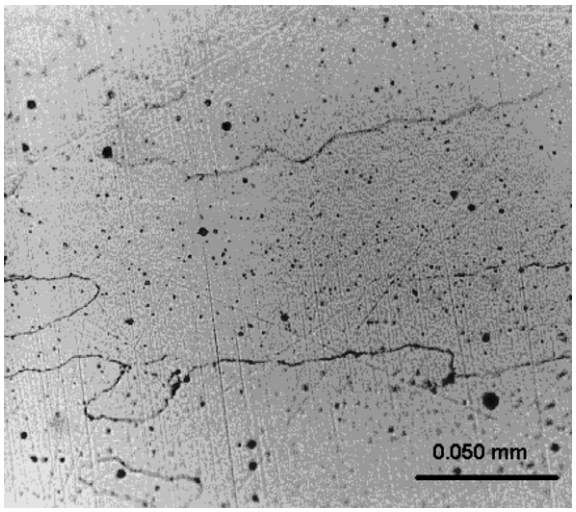

Fig. 7. Metallographic section along the *T*–*S* plane, after annealing. Note the quasi absence of the δ phase compared with Fig. 6 and the wavy grain boundaries.

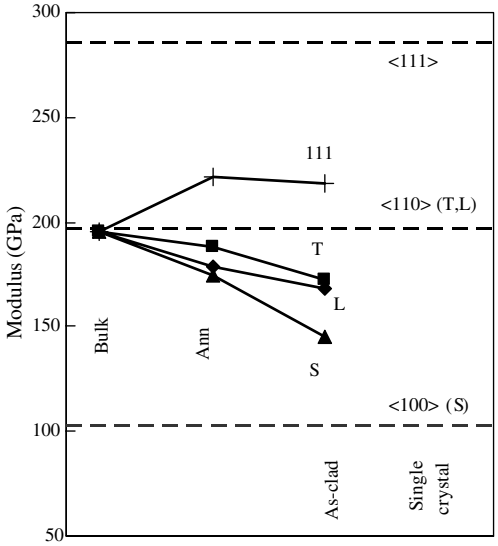

Fig. 8. Dependence of the moduli on orientation and material condition. The broken horizontal lines represent the calculated values for the indicated single-crystal directions. From left to right, the moduli for isotropic, clad-and-annealed and as-clad material are shown.

from the isotropic to the clad-and-annealed condition a modulus change occurs for all orientations. Going further to the as-clad condition causes a change of the same order of magnitude in the *L*, *T* and *S* directions, while for the ⟨1 1 1⟩ direction no significant change is observed.

6. Discussion

6.1. Texture

The XRD patterns clearly show the existence of a strong texture in the cladding upper layer and a similar but less pronounced texture in the lower layer. These textures are most probably due to the heat flow during solidification which is expected to have occurred mainly parallel to the *S* direction. Their different strengths are probably due a different cooling rate of both layers, due to different preheating or cladding conditions. The type of texture, i.e. ⟨1 0 0⟩ parallel to the heat flow, is similar to the one, which has been observed in austenitic welds [5,6]. The texture within the cladding plane may be due to anisotropic heat flow linked with the movement of the cladding head.

6.2. Moduli for the clad-and-annealed condition. Texture effect

The difference between the moduli measured along the *L*, *T*, *S* and ⟨1 1 1⟩ directions and the bulk modulus is clearly due to the observed texture. This can be seen from Fig. 8 which shows the relation between the measured moduli and the calculated moduli for the corresponding crystallographic directions, according to the observed texture. It can be seen that there is a good ranking agreement, i.e. a direction with a low measured modulus corresponds with a low modulus single-crystal direction (e.g. *S* and ⟨1 0 0⟩) and vice versa. The deviations of the measured values from the calculated single crystal ones are most probably due to the imperfection of the texture.

6.3. Moduli for the as-clad condition. Effect of the δ phase

The main difference between the as-clad and the annealed condition must have been caused by the dissolution of the δ phase since the texture in the austenite phase was shown to be unaffected by the annealing treatment. The effect of the δ phase on the elastic moduli clearly depends on the orientation as can be seen from Fig. 8. Some possible causes for the δ phase effect are considered below.

6.3.1. Elastic effect

The elastic constants of bcc iron [14], Fe–19%Cr [15] and austenite [7] are very close, but both austenite and ferrite are anisotropic as shown by the modulus dependence on the crystallographic direction. In a textured material the overall modulus will therefore depend on the orientation relationship between both phases and on the direction considered. In the top layer the δ phase has the same texture as the austenite and the effect will be nil because of the similarity of the elastic constants. In the bottom layer the δ phase is oriented randomly relative to the austenite. Local effects are expected but they will probably average out over a large number of austenite grains. This conclusion is supported by considering that the large modulus decrease occurring in the *S* direction (around 14%) is hard to explain by a low ferrite modulus in view of the small volume fraction of the δ phase.

6.3.2. Composition effect due to dissolution of the δ phase

Since literature data show that molybdenum, chromium and nickel have a very small influence on the bulk modulus

of austenitic steels [2,3,9,10] a composition change can be excluded as a cause of the observed modulus changes.

6.3.3. Strain effect caused by the difference in thermal expansion between ferrite and austenite

The thermal expansion coefficient of ferritic steels is around 12×10^{-6}/K while for austenitic steels it is around 18×10^{-6}/K [2]. From the melting point (about 1400 °C) to room temperature, this results in a difference of linear shrinkage of 0.8%. It can therefore be expected that the δ phase dendrites will be surrounded by strain fields, each consisting of dislocations with a specific Burgers vector. As a consequence of the texture, these Burgers vectors will have fixed orientations relative to the macroscopic *L*, *S*, *T* and ⟨1 1 1⟩ directions. It has been shown theoretically that if suitably orientated dislocations are present, dislocation movement during 'elastic' straining may decrease the elastic modulus by 15% [16]. This was confirmed by small-strain torsion experiments on copper showing a modulus decrease of 17% [17]. On the other hand, in 10% cold worked copper and aluminum a decrease of only 1–2% is observed [14]. In this case the extensive cold work may have limited the amount of elastic dislocation movement. Although the presence of specific strain fields may explain the observed modulus decreases and their dependence on the orientation, some problems remain. As for the elastic effect discussed above, it should be considered that the volume occupied by the δ phase is rather small and therefore unlikely to affect the whole austenite matrix. The fact that the modulus does not change in the ⟨1 1 1⟩ direction is not readily explained. Furthermore, the observation that deliberate bending and straightening (plastic strain up to 2%) does not affect the modulus is hard to reconcile with the strain field hypothesis. Finally, an explanation should be given for the observation that the impulse excitation measurements show no effect upon annealing. This may be because this method uses extremely low stresses, which are unlikely to cause any dislocation movement. Its results therefore do not contradict the strain field hypothesis.

In conclusion, it should be stated that, at present, none of the mechanisms discussed above are fully satisfactory and that a more detailed analysis would be required to give a quantitative explanation of the δ phase effect.

7. Conclusions

A method for the determination of the static Young modulus by means of small cantilever bend test pieces has been developed. Using this method on an RPV cladding showed that in the as-clad condition the moduli along the *L*, *T*, *S* and ⟨1 1 1⟩ directions deviate from the bulk value of 195 GPa by respectively −15, −13, −25 and +12%. After dissolving the δ phase by an annealing treatment, the deviations for *L*, *T* and *S* are approximately halved, while in the ⟨1 1 1⟩ direction no change occurs.

From XRD diffraction patterns it was found that both the austenite and the ferrite show a solidification texture with ⟨1 0 0⟩//*S* and ⟨1 1 0⟩//*L*. This texture is more pronounced in the top layer.

For the annealed condition the deviations of the moduli from the bulk modulus are explained by the solidification texture. The difference between the moduli in the as-clad and the annealed conditions is also orientation dependent and is attributed to an effect caused by the δ phase.

Acknowledgements

The authors want to thank Dr L. Malerba and Dr M. Konstantinovic for useful discussions during the preparation of this article.

References

[1] Annual Book of ASTM Standards, ASTM Standard E1876-01, Standard Test Method for Dynamic Young's Modulus and Poisson's Ratio by Impulse Excitation of Vibration, 2001.
[2] Metals Handbook, Properties and Selection: Irons, Steels and High Performance Alloys, tenth ed., vol. 1, ASM International, 1990.
[3] C.W. Wegst, Stahlschlüssel, Verlag Stahlschlüssel Wegst, Marbach, 1998.
[4] An Investigation of the Transferability of Master Curve Technology to Shallow Flaws in Reactor Pressure Applications, NESC-IV Project (EU-Network for Evaluating Structural Components), September 2005, 22–23.
[5] D.S. Kupperman, K.J. Reimann, IEEE Trans. Son. Ultrason. SU-27 (1) (1980) 7.
[6] B.R. Dewey, L. Adler, R.T. King, K.V. Cook, Exp. Mechan. 17 (1977) 420.
[7] H.M. Ledbetter, Brit. J. NonDestr. Test. 34 (1981) 286.
[8] H.M. Ledbetter, Metal Sci. 14 (1980) 595.
[9] H.M. Ledbetter, S.A. Kim, J. Mater. Res. 3 (1988) 40.
[10] S. Kim, H. Ledbetter, Y.Y. Li, J. Mater. Sci. 29 (1994) 5462.
[11] S. Timoshenko, D.H. Young, Elements of Strength of Materials, 4th Ed., D. Van Nostrand Company, Princeton, 1962.
[12] W.C. Young, R.G. Budynas, Roark's Formulas for Stress and Strain, 7th Ed., McGraw Hill, New York, 2002.
[13] G.E. Dieter, Mechanical Metallurgy, 3rd Ed., McGraw-Hill Series in Materials Science and Engineering, New York, 1986.
[14] W.J. McGregor Tegart, Elements of Mechanical Metallurgy, The Macmillan Company, New York, 1966.
[15] H. Masumoto, M. Kikuchi, Trans. JIM 12 (1971) 90.
[16] J. Friedel, Dislocations, International Series of Monographs on Solid State Physics, vol. 3, Pergamon, 1964.
[17] M.J. Druyvesteyn, O.F.Z. Schannen, E.C.J. Swaving, Physica 25 (1959) 1271.